Modified-Bloch-equation description of EPR transient nutations and free induction decay in solids

2001 J. Phys.: Condens. Matter 13 3475

(http://iopscience.iop.org/0953-8984/13/14/319)

INSTITUTE OF PHYSICS PUBLISHING JOURNAL OF PHYSICS: CONDENSED MATTER

J. Phys.: Condens. Matter **13** (2001) 3475–3489 www.iop.org/Journals/cm PII: S0953-8984(01)22179-1

Modified-Bloch-equation description of EPR transient nutations and free induction decay in solids

N Ya Asadullina, T Ya Asadullin[1] and Ya Ya Asadullin

Kazan State Technical University, Department of General Physics, Karl Marx street 10, Kazan 420111, Russia

E-mail: atimur@physics.ktsu-kai.ru (T Ya Asadullin)

Received 20 February 2001

Abstract

Based on the experimental work by Boscaino *et al* on the EPR transient nutations (TNs) and free induction decay (FID) in solids, we propose the modified Bloch equations (MBEs). In addition to the Tomita expression for power-dependent parameter T_{2u}, we give an original phenomenological expression for power-dependent parameter T_{2v} and tuning Δ. Both analytical (in the form of a Torrey solution with these parameters) and numerical solutions of MBE are obtained for TN and for different FID regimes with very good agreement between theory and experiment. We also discuss the meaning and role of the instantaneous diffusion mechanism in the transient pulse experiments.

1. Introduction

In a series of papers [1–6], Boscaino and his co-workers have reported several important experimental results on the EPR transient nutations (TNs) and free induction decay (FID) in solids. They have also given an exhaustive qualitative discussion of their results and the literature on the subject to date. The purpose of this paper is to present a quantitative description of the Boscaino results as they do not agree with the existing theoretical predictions.

As is known [1–3, 7], the nutational response monitors the time evolution of a system, initially at thermal equilibrium, toward a new stationary state under the action of an intense resonant field $H_{mw}(t) = 2H_{mw}\cos(\Omega t)$. The FID effect [4–6, 8, 9] is the emission of radiation ensuing from the abrupt interruption of the pump field.

To describe the above effects and other resonance and relaxation processes in magnetic resonance and in optics, the Bloch equations are widely used. In the rotating with frequency Ω reference frame, these equations are

$$\dot{u} + \Delta v + \frac{u}{T_{2u}} = 0$$

$$\dot{v} - \Delta u - \chi\omega + \frac{v}{T_{2v}} = 0$$

[1] Corresponding author.

0953-8984/01/143475+15$30.00

$$\dot{w} + \chi v + \frac{(w - w_0)}{T_1} = 0 \tag{1}$$

and follow from the density-matrix equations of motion for a two-level quantum system. In the case of the magnetic resonance, u, v and w are the components of the homogeneous spin-packet magnetization. Ordinary Bloch equations (OBEs) properly (1) include two constant phenomenological relaxation parameters, T_1 and $T_{2u} = T_{2v} = T_2 = \Gamma_2^{-1}$, the power-independent tuning parameter $\Delta = \omega_0 - \Omega$, where ω_0 is the transition frequency, and the induced Rabi frequency $\chi = \gamma H_{mw}$, where γ is the gyromagnetic ratio.

In experiments [1–6], whose results we propose to discuss below, one deals with the inhomogeneous spin systems. Hence, one assumes an inhomogeneously broadened resonance line with a Gaussian profile and a standard deviation σ:

$$g(\omega) = (2\pi)^{-1/2}\sigma^{-1}\exp(-\omega^2/2\sigma^2) \tag{2}$$

where $\omega = \omega_0 - \omega_{00}$ measures the spectral distance of the generic spin (ω_0) from the mean frequency ω_{00}. To obtain the nutation signal of the whole system $V(t)$, one has to solve equations (1) for the generic spin ω and integrate over the distribution $g(\omega)$. The approximate solution, valid under the conditions (i) centre excitation and (ii) $T_1 \gg T_2$; (iii) $\chi \gg T_1^{-1}$, Γ_2, is given by [2, 7]

$$V_B(t) \propto J_0(\chi t)\exp(-\Gamma_B t) \qquad \Gamma_B = 1/2T_2. \tag{3}$$

Here subscript B indicates belonging to the ordinary Bloch model with constant T_1 and T_2. The zeroth-order Bessel function $J_0(\omega t)$ (as in equation (3)) describes the reversible damping caused by the inhomogeneous broadening [7]. The second factor shows that the irreversible decay due to the relaxation interactions is a single exponential function with the constant decay rate.

In contrast to this theoretical prediction, the observed decay [1–3] is *faster* than expected and depends on the driving-field intensity. The power dependence of the decay rate Γ is well described by a linear dependence of Γ on the induced Rabi frequency $\chi = \gamma H_{mw}$ [2]:

$$\Gamma = \alpha + \beta\chi. \tag{4}$$

Furthermore, parameter β increases on increasing spin concentration n_0 [3].

In the case of FID experiments [4–6], it was found that the decay of the signal also depends on the driving-field intensity but is much *slower* than expected on the basis of the OBE.

Similar results are observed in experiments on optical FID [10, 11]. Thus, it follows from experiments [1–6, 10, 11] that the phenomenological parameter T_2 in (1) is power dependent.

To explain the observed experimental results, several possible origins of the amplitude-dependent decay have been considered. In particular, the non-Bloch behaviour of the FID rate has been ascribed to the fluctuations of the resonance frequency ω_{0i} of the active centres and/or of the field source [12–14]. Shakhmuratov *et al* [15] proposed the modified Bloch equations (MBEs) based on the assumption that the active centres experience not only the coherent driving field but also a stochastic field. The stochastic field in turn is supposed to depend linearly on the amplitude of the coherent field.

Our approach to the decay processes of the TN and FID to be considered below is the *opposite* to that in the previous publications [12–15] (see also other references therein). Namely, we emphasize that in all the transient phenomena under consideration we are dealing with an essentially coherent exciting field [3] and detect a coherent response of the system of coherently excited spins/atoms. Of course, any kinds of interaction in the system reduce the coherence and lead to damping. In the case of Boscaino experiments, the amplitude-dependence of the decay rate $\Gamma(\chi)$ arises from the magnetic dipole–dipole interaction of active spins. More precisely, the decay rate arises from the interaction of an active spin with

the rotating in the perpendicular to the applied field $\boldsymbol{H}_0$ plane components of the local dipolar field $H_{loc}(u, v)$ of the other active spins:

$$H_{loc}(u, v) = |H_\perp(u, v)| \sim \left[\sum (u_i^2 + v_i^2)\right]^{1/2}$$

where u_i, v_i are functions of χ. In its turn, H_{loc} causes changes in spin orientation. Because of the inhomogeneous broadening, each spin has its own resonance frequency and phase so that the net effect of the local field is noisy in nature and led to the homogeneous broadening characterized by $\Gamma(\chi)$. Nevertheless, $\Gamma(\chi)$ is expressed in terms of nonrandom functions $u_i(t)$ and $v_i(t)$. In the next section we give explicit expressions for the intensity-dependent parameters T_{2u}, T_{2v} and Δ forming the basis for our modified Bloch equations (MBEs) (1). Sections 3 and 4 are devoted to theoretical and numerical study of TN and FID respectively on the basis of MBE. The relation of parameters $T_{2v}(\chi)$ and $\Delta(\chi)$ to the instantaneous diffusion (ID) mechanism [16] as well as other results of previous sections are discussed briefly in section 5.

2. Modified Bloch equations

In accordance with experiments [1–3], we have to take into account the power dependence of T_{2u}, T_{2v} and of the tuning parameter Δ, that is of the transition frequency ω_0. For an inhomogeneously broadened system one has

$$\Delta = \Delta_0 + \omega + \Delta\omega \tag{5}$$

where $\Delta_0 = \omega_{00} - \Omega$ and ω_{00} is the central frequency of the inhomogeneously broadened line. In the case of centre excitation (as in experiments [1–6] and accepted here), $\Delta_0 = 0$. Finally, $\Delta\omega$ gives the intensity-dependent shift of the transition frequency due to change in the z-component of the local magnetic field. Indeed, driving field $H_{mw}(t)$ changes the z-components of the magnetic moments of the paramagnetic centres (in experiments [1–6] one deals with centres of effective spin $S = 1/2$) and, as a consequence, it changes the z-component of the magnetization M_z:

$$\begin{aligned}
&\Delta M_z(t) = M_0 - M_z(t) = \int_{-\infty}^{\infty} [w_0 - w(\Delta, t)]\Delta n_2(\Delta, t)\,\mathrm{d}\Delta \\
&\Delta n_2(\Delta, t) = \left(\frac{n_0}{2} - n_{20}\right)\frac{S(\Delta, \chi)}{1 + S(\Delta, \chi)}\{1 - \exp[-(1 + S(\Delta, \chi))t/T_{10}]\}g(\Delta) \\
&S(\Delta, \chi) = \frac{1}{4}\frac{T_1\Gamma_{2v}\chi^2}{\Delta^2 + \Gamma_{2v}^2/4} \qquad T_{10}^{-1} = w_{21} + w_{12} = T_1^{-1}.
\end{aligned} \tag{6}$$

Here $\Delta n_2(\Delta, t) = n_2(\Delta, t) - n_{20}(\Delta)$ is the change in the spectral concentration of the excited spins $n_2(\Delta, t)$ (with initial equilibrium value $n_{20}(\Delta)$) during the excitation by $H_{mw}(t)$ and obtained as a solution of the rate equation

$$\begin{aligned}
&\dot{n}_2(\Delta, t) = -(w_{21} + W_{21})n_2(\Delta, t) + (w_{12} + W_{12})n_1(\Delta, t) \\
&n_1(\Delta, t) + n_2(\Delta, t) = n(\Delta) = n_0 g(\Delta) \qquad n_1 + n_2 = n_0.
\end{aligned} \tag{7}$$

Here w_{21} is the transition probability per second for a spin from excited level 2 to ground level 1, w_{12} is the probability for the reverse process, $W_{21} = 2\pi\chi^2 g_L(\omega)$ and W_{12} are the probabilities for induced transitions $1 \leftrightarrow 2$, and $g_L(\omega)$ is the usual Lorentzian profile. In equation (6) $S(\Delta, \chi)$ is the spectral saturation parameter. The definition of relaxation rate $\Gamma_{2v} = T_{2v}^{-1}$ is discussed below. With the driving field switched off, the system is relaxed to the equilibrium state with the relaxation time T_{10} which we identify with T_1 in equations (1).

The change in the demagnetizing field $\Delta H_{demag} \sim \Delta M_z$ leads to the time-dependent change of the Zeeman frequency as follows:

$$\Delta\omega(t) = a_\omega \Delta M_z(t) \tag{8}$$

where a_ω is a parameter.

As noted in the introduction, the transverse components of the magnetization contribute to the intensity-dependent damping. One has to distinguish between the damping for the u-component (along which field $H_{mw}(t)$ is directed) described by decay rate $\Gamma_{2u} = T_{2u}^{-1}$ and that for the v-component with decay rate $\Gamma_{2v} = T_{2v}^{-1}$. It is shown by Redfield [17] that H_{mw} suppresses the phase relaxation process for the u-component. Following [18], we have

$$\Gamma_{2u} = \frac{\Gamma_0}{1 + r^2\chi^2} + \frac{1}{2T_1} \tag{9}$$

for closed systems, and

$$\Gamma_{2u} = \frac{\Gamma_0}{1 + r^2\chi^2} + \frac{1}{T_1} \tag{10}$$

for open systems. Here $\Gamma_0 = T_2^{-1}$ is the relaxation rate at small values of H_{mw} and r a parameter, associated with the correlation time of dipole–dipole interactions [18]. Note, however, that the relaxation process associated with Γ_{2u} is of little importance for TN, as will be seen below.

While Γ_{2u} decreases with increasing H_{mw}, decay rate Γ_{2v} *increases* due to the building up of the transverse component of dipole moments

$$m_\perp(\Delta, t) = [u^2(\Delta, t) + v^2(\Delta, t)]^{1/2} \tag{11}$$

during the excitation process. We approximate Γ_{2v} by the following expression:

$$\Gamma_{2v} = \Gamma_0\left[1 + \frac{1}{(2)T_1\Gamma_0}\right] + a_\Gamma \int |m_\perp(\Delta, t)|\Delta n_2(\Delta, t)\,\mathrm{d}\Delta$$
$$\Delta n_2(t) = \int \Delta n_2(\Delta, t)\,\mathrm{d}\Delta. \tag{12}$$

The first term on the right-hand side of equation (12) describes the contribution to the damping from the thermally excited spins and from the spin-lattice interaction, the second being due to the coherently excited spins. For $\chi \to 0$, Γ_{2v} coincides with Γ_{20} (9) or (10).

It is obvious from equations (5), (7), (10) and (11) that parameters Δ and Γ_{2v} are dependent on $u(t)$, $v(t)$ and $w(t)$; therefore, the modified Bloch equations are inherently nonlinear.

3. Transient nutations

3.1. Theory

It follows from (6) and (12) that required parameters Γ_{2v}, $\Delta n_2(\Delta, t)$ and variables $u(t)$, $v(t)$ are interrelated. We construct $\Delta n_2(\Delta, t)$, $\Delta n_2(t)$, $\Delta\omega(t)$ and $\Gamma_{2v}(t)$ by the method of iteration. In the zeroth approximation ($k = 1$), for $u(t)$, $v(t)$ and $w(t)$ we use the well known Torrey solution [7] corresponding to conditions (i)–(iii) in the introduction. With equations (9) or (10) for Γ_{2u}, $\Gamma_{2v} = \Gamma_0$ and $\Delta = \omega$, the solution is given by

$$u = w_0\left\{\frac{c}{c^2 + \Gamma_{2u}T_1} + \frac{c}{s}\left(1 - \frac{s}{c^2 + \Gamma_{2u}T_1}\right)\exp\left(-\frac{c^2 + \Gamma_{2u}T_1}{s}\frac{t}{T_1}\right)\right.$$
$$\left. -\frac{c}{s}\exp\left(-\frac{1}{2}\left(\Gamma_{2v} + \Gamma_{2u} - \frac{\Gamma_{2u} - T_1^{-1}}{s}\right)t\right)\cos(\sqrt{s}\chi t)\right.$$

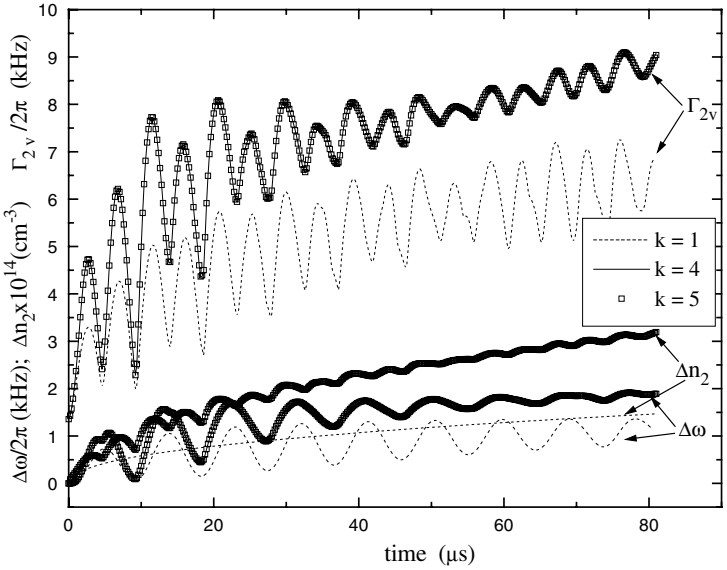

Figure 1. Excited spin concentration, $\Delta n_2(t) = n_2(t) - n_{20}$, resonance frequency shift, $\Delta\omega(t)$, and damping parameter, $\Gamma_{2v}(t)$, versus excitation time, t. The Rabi frequency $\chi = 2\pi \times 107$ kHz, k is the iteration number. For other parameters relevant to figures 1–4 see the text in section 3.2.

$$
\begin{aligned}
&+\frac{c}{s^{3/2}\chi}\left[\frac{1}{2s}\left(c^2\left(\frac{2}{T_1}-\Gamma_{2v}-\Gamma_{2u}\right)+2\Gamma_{2u}-\frac{1}{T_1}-\Gamma_{2v}\right)-\frac{1}{T_1}\right]\\
&\times\exp\left(-\frac{1}{2}\left(\Gamma_{2v}+\Gamma_{2u}-\frac{\Gamma_{2u}-T_1^{-1}}{s}\right)t\right)\sin(\sqrt{s}\chi t)\Bigg\}\\
v = w_0\Bigg\{&-\frac{\Gamma_{2u}}{\chi(c^2+\Gamma_{2u}T_1)}-\frac{c^2(\Gamma_{2u}T_1-1)}{\chi T_1 s}\left(\frac{1}{s}-\frac{1}{c^2+\Gamma_{2u}T_1}\right)\exp\left(-\frac{c^2+\Gamma_{2u}T_1}{s}\frac{t}{T_1}\right)\\
&+\frac{1}{s\chi}\left[\frac{c^2}{s}\left(\Gamma_{2u}-\frac{1}{T_1}\right)+\frac{1}{T_1}\right]\exp\left(-\frac{1}{2}\left(\Gamma_{2v}+\Gamma_{2u}-\frac{\Gamma_{2u}-T_1^{-1}}{s}\right)t\right)\\
&\times\cos(\sqrt{s}\chi t)-\frac{1}{s^{1/2}}\exp\left(-\frac{1}{2}\left(\Gamma_{2v}+\Gamma_{2u}-\frac{\Gamma_{2u}-T_1^{-1}}{s}\right)t\right)\sin(\sqrt{s}\chi t)\Bigg\}\\
w = w_0\Bigg\{&\frac{c^2}{(c^2+\Gamma_{2u}T_1)}+\frac{c^2}{s}\left(1-\frac{s}{c^2+\Gamma_{2u}T_1}\right)\exp\left(-\frac{c^2+\Gamma_{2u}T_1}{s}\frac{t}{T_1}\right)\\
&+\frac{1}{s}\exp\left(-\frac{1}{2}\left(\Gamma_{2v}+\Gamma_{2u}-\frac{\Gamma_{2u}-T_1^{-1}}{s}\right)t\right)\cos(\sqrt{s}\chi t)\\
&+\frac{1}{s^{3/2}\chi}\left[\frac{1}{2s}\left(c^2\left(\Gamma_{2v}+3\Gamma_{2u}-4\frac{1}{T_1}\right)+\Gamma_{2v}-\frac{1}{T_1}\right)+\frac{1}{T_1}\right]\\
&\times\exp\left(-\frac{1}{2}\left(\Gamma_{2v}+\Gamma_{2u}-\frac{\Gamma_{2u}-T_1^{-1}}{s}\right)t\right)\sin(\sqrt{s}\chi t)\Bigg\}. \qquad (13)
\end{aligned}
$$

Here $c = \Delta/\chi = \omega/\chi$, $s = 1 + c^2$.

Solution (13) is used in equations (6), (8), (11) and (12) to obtain expressions for $\Delta n_2(\Delta, t)$, $\Delta n_2(t)$, $\Delta\omega(t)$ and $\Gamma_{2v}(t)$; the latter are, in its turn, inserted into equations (13) and so on. Really, the expressions for $\Delta n_2(t)$, $\Delta\omega(t)$ and $\Gamma_{2v}(t)$ get their final form after

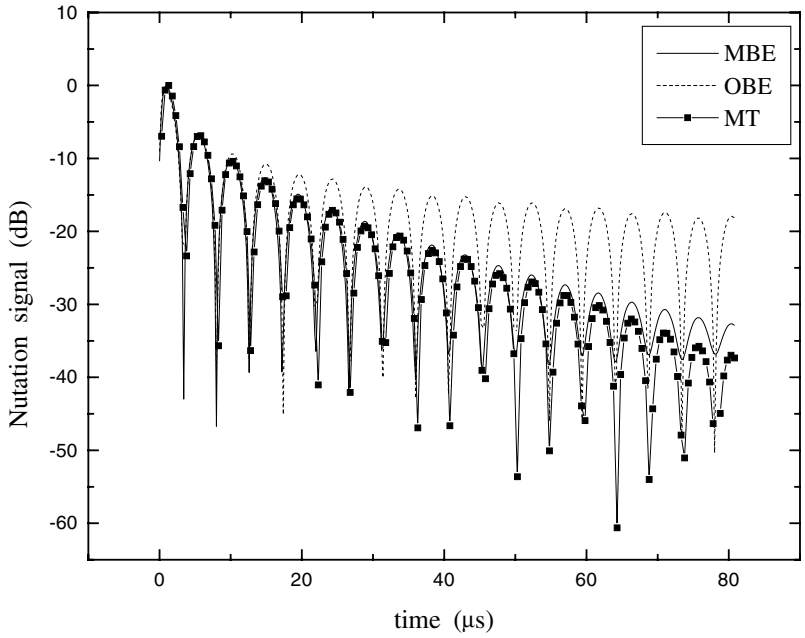

Figure 2. Calculated curves of the nutational response $S(t) \propto |V(t)|$ at Rabi frequency $\chi = 2\pi \times 107$ kHz. The full line is the numerical solution of the modified Bloch equations (1); the line with symbols is the modified Torrey solution (13) and the dotted line is numerical solution of the ordinary Bloch equations.

five cycles and do not vary further (see figure 1). Note that the time dependence of $\Delta\omega(t)$ is modulated with the Rabi frequency whereas for $\Delta n_2(t)$ and $\Gamma_{2v}(t)$ one has the double Rabi frequency. Expressions (13) obtained in such a way represent the modified analytic Torrey solution and will be used below in FID studies. Remember, however, that this solution is subject to conditions (i)–(iii) above and is only an approximate one.

The MBE (1) with thereby obtained parameters $\Gamma_{2u}(t)$, $\Gamma_{2v}(t)$ and $\Delta\omega(t)$ are further solved numerically for various values of the Rabi frequency χ. The experimentally observable signal is $S(t) \sim (U^2(t) + V^2(t))^{1/2} \approx |V(t)|$, where $U(t)$ and $V(t)$ are obtained by integration of $u(t)$ and $v(t)$ over the inhomogeneous line profile. Note that, as turns out from the numerical calculations, though $U(t) \neq 0$, it is smaller by two or three orders than $V(t)$.

3.2. Numerical calculations

Examples of the nutational response $S(t)$ are given in figure 2. The full curve shows the TN signal at $\chi = 2\pi \times 107$ kHz obtained as a numerical solution of the MBE (1) with parameters $\Gamma_{2u}(t)$, $\Gamma_{2v}(t)$ and Δ given in the preceding subsection. To obtain this result, figure 1, and other results of this section, the following values of the parameters were used: $a_\omega = 1.78 \times 10^{-9}$ cm^{-3} c^{-1}, $a_\Gamma = 1.2 \times 10^{-8}$ cm^{-3} c^{-1}, $r^2 = 2 \times 10^{-9}$ c^2. Unfortunately, in references [2, 5, 19, 20] there is considerable scatter in the values of parameters T_2, σ and n_0 presumably relevant to one and the same sample with $T_1 = 5 \times 10^{-3}$ c. Here we take $T_2 = \Gamma_0^{-1} = 1.2 \times 10^{-4}$ c, $\sigma = 2\pi \times 0.25$ MHz ($T_2^* = \sigma^{-1} = 0.63$ μs), $n_0 = 4 \times 10^{16}$ cm^{-3} characteristic for sample N1 in [2] and the equilibrium value of the polarization $p_0 = 3.3687 \times 10^{-2}$.

The dotted curve in figure 2 is the TN signal obtained as a numerical solution of the OBE and the line with symbols is the response obtained by use of the modified Torrey solution (13). It is seen from figure 2 that the decay of the MBE response is considerably *faster* than that of the OBE response and the modified Torrey signal decayed approximately with the same rate as the MBE response.

Further, for the MBE response we have examined the decay function $K(t)$ [2] representing the effect of the irreversible relaxation and for the ordinary Bloch model given by $K(t) = \exp(-\Gamma_B t)$ (3). As in [2], we considered only the maxima of the signal (see figure 2): the values S_i ($i = 1, N$; N is the number of maxima) of the maxima were compared to the extremes $|J_0|_i$ (absolute values of maxima and minima) of the zeroth-order Bessel function. The obtained values of $K_i = S_i/|J_0|_i$ were arranged in a plot of K versus t, as shown by symbols in figure 3 for two values of χ. One sees that the decay function $K(t)$ is well described by a single exponential as $K(t) = \exp(-\Gamma t)$, excepting the first maximum. The departure of the first maximum from the straight line (noted also in [2]) is caused by the fact that the first maximum of the signal appears at $t > 0$, while the first maximum of $J_0(\chi t)$ is at $t = 0$. The calculated decay rate Γ depends on the input power: in figure 3 we have $\Gamma/2\pi = 1.38$ kHz for $\chi/2\pi = 21$ kHz and $\Gamma/2\pi = 3.7$ kHz for $\chi/2\pi = 107$ kHz, in good agreement with experiment [2].

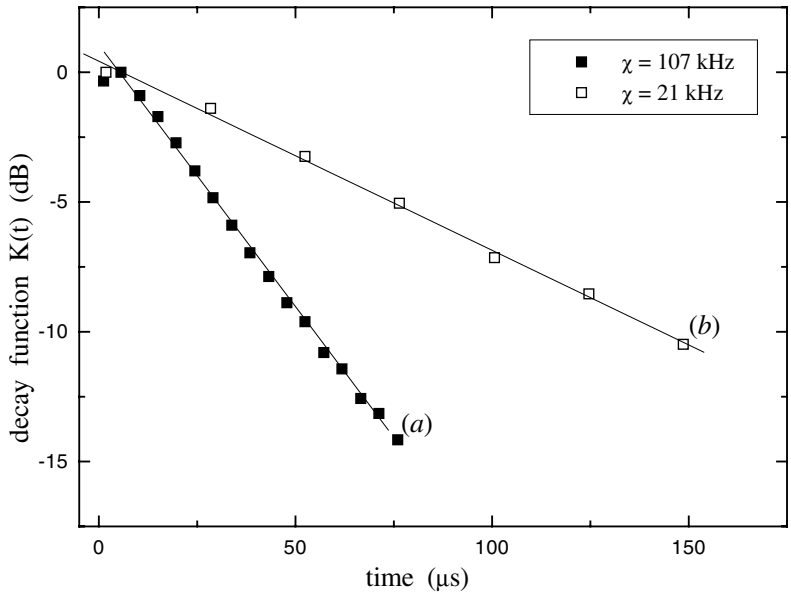

Figure 3. Calculated decay function $K(t)$. (*a*) Solid squares are calculated values, as determined from the solid line of figure 2 by points (at the maxima) for $\chi = 2\pi \times 107$ kHz; (*b*) open squares are the same for $\chi = 2\pi \times 21$ kHz. The lines plot the single exponential functions $K(t) = \exp(-\Gamma t)$, the best fit the calculated points, excluding the initial points (see text). One gets $\Gamma = 2\pi \times 3.7$ kHz (*a*) and $\Gamma = 2\pi \times 1.38$ kHz (*b*).

We calculate $K(t)$ at different power levels in a broad range of experimentally available values of χ [2] with the result that $K(t)$ in the whole range is well described by a single exponential with the intensity-dependent decay rate $\Gamma = \Gamma(\chi)$. It is seen from figure 4 that this dependence is well described as a linear function of the induced Rabi frequency χ, equation (4), again in good agreement with experiment [2]. The calculated values of the

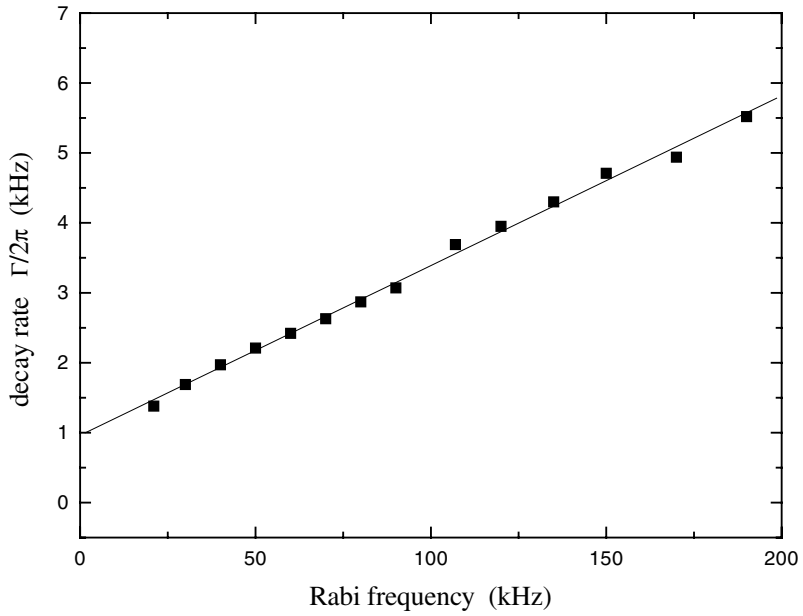

Figure 4. Calculated TN decay rate, Γ, versus Rabi frequency, χ, for sample no 1 of [2]. Dots are calculated points; solid line is the best fit straight line: $\Gamma = \alpha + \beta\chi$. $\alpha/2\pi = 0.96$ kHz; $\beta = 0.024$.

quantities α and β in equation (4) are $\alpha = 2\pi \times 0.96$ kHz, $\beta = 0.024$, while experiment [2] gives $\alpha = 2\pi \times (0.78 \pm 0.08)$ kHz, $\beta = 0.024 \pm 0.1$.

4. Free-induction decay

4.1. Theory

FID response strongly depends on the excitation-pulse amplitude and duration t_p, on the inhomogeneous broadening of the resonance line etc. Schenzle *et al* [21] theoretically predicted and Kunitomo *et al* [22] verified by NMR experiments that FID exhibits amplitude oscillations if the following conditions are satisfied: (1) the inhomogeneous line width σ is very large compared with the homogeneous one, (2) the pulse area $\chi t_p \geqslant 2\pi$ and (3) $\chi < \sigma$. Further, it was shown [21, 23] that with a preparation pulse of finite duration t_p, the FID signal lasts only for an additional period t_p. Bearing the finite-pulse-prepared FID in mind, we observe from figure 2 that description of the TN experiments by the modified Torrey solution (13) is quite satisfactory. Therefore, expressions (13) can be considered as an initial value ($u^{(0)}(t_p)$, $v^{(0)}(t_p)$, $w^{(0)}(t_p)$) for the FID prepared by an exciting pulse of any length t_p, if one substitutes t_p for t there.

On the other hand, in experiments [4–6] the FID effect was observed after excitation of the spin system to the saturated state. Hence, the initial value of the Bloch vector for a spin packet in the FID process is given by the steady-state solution of equation (1):

$$u^{(0)} = \frac{\Delta\chi w_0 T_{2u} T_{2v}}{D} \qquad v^{(0)} = -\frac{\chi w_0 T_{2v}}{D} \qquad w^{(0)} = \frac{(1 + \Delta^2 T_{2u} T_{2v}) w_0}{D} \tag{14}$$

$$D = 1 + \Delta^2 T_{2u} T_{2v} + \chi^2 T_1 T_{2v}.$$

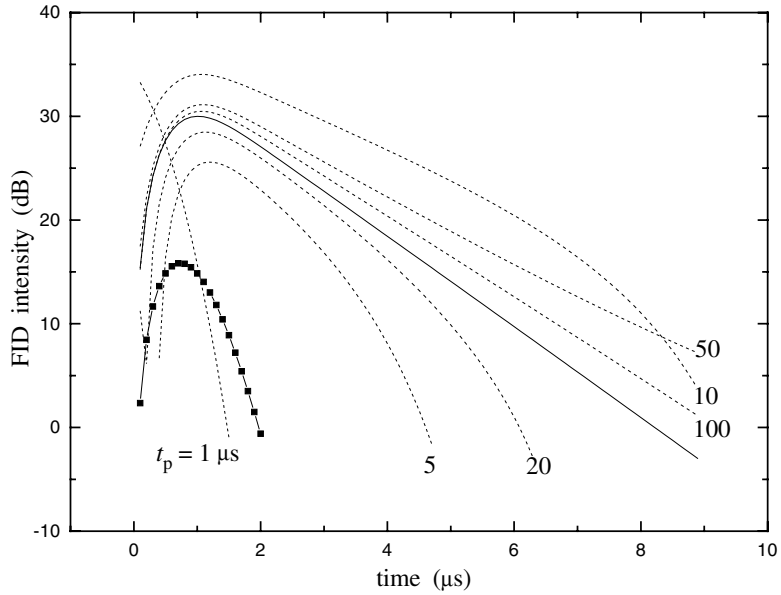

Figure 5. FID responses calculated in the MBE model prepared by pulses of different lengths t_p. $\chi = 2\pi \times 54$ kHz. Full and line–symbol curves are steady-state prepared FID responses in MBE and OBE models respectively.

Note that the first terms in the curly brackets of equations (13) are nothing more than the limiting case of equations (14) under conditions (i)–(iii).

After the switching-off the exciting-pulse at time $t = 0$, free decay of the transverse components for a spin packet in our modified Bloch model is described by

$$u(\Delta, t) = (u^{(0)}(t_p)\cos(\Delta t) - v^{(0)}(t_p)\sin(\Delta t))\exp(-t/T_{2v})$$
$$v(\Delta, t) = (v^{(0)}(t_p)\cos(\Delta t) + u^{(0)}(t_p)\sin(\Delta t))\exp(-t/T_{2v}). \tag{15}$$

In expressions (14) and (15), $T_{2u} = 1/\Gamma_{2u}$ is still given by formulae (9) or (10), but in the definition (12) of Γ_{2v} now we have $\Delta n_2(\Delta, t_p)$, $\Delta n_2(t_p)$ and, in particular, (see equation (6))

$$\Delta n_2(\Delta, t_p \to \infty) = \left(\frac{n_0}{2} - n_{20}\right)\frac{S(\Delta\chi)}{1 + S(\Delta, \chi)}g(\Delta). \tag{16}$$

Again, expressions for $\Delta n_2(\Delta, t_p)$, $\Delta n_2(t_p)$, $\Delta\omega(t_p)$ and $\Gamma_{2v}(t_p)$ are obtained by iteration. The final expression for the FID signal is given by integration of $u(\Delta, t)$ and $v(\Delta, t)$ over distribution $g(\Delta)$ (2).

4.2. Numerical calculations

First we consider the FID response for the pulse area smaller than 2π. Figure 5 shows the free induction decay after excitation by pulses of different length with a reference Rabi frequency $\chi = 2\pi \times 54$ kHz [5]. For short pulse length $t_p \cong 1$ μs the signal amplitude only increases quickly from large negative values through zero to small positive ones, so the observable intensity decreases at times $t \cong 1.5$ μs. With increasing t_p, FID intensity initially increases to a maximum before decaying monotonically for larger t. For short (relative to T_2) $t_p = 1$–50 μs the decay is not exponential.

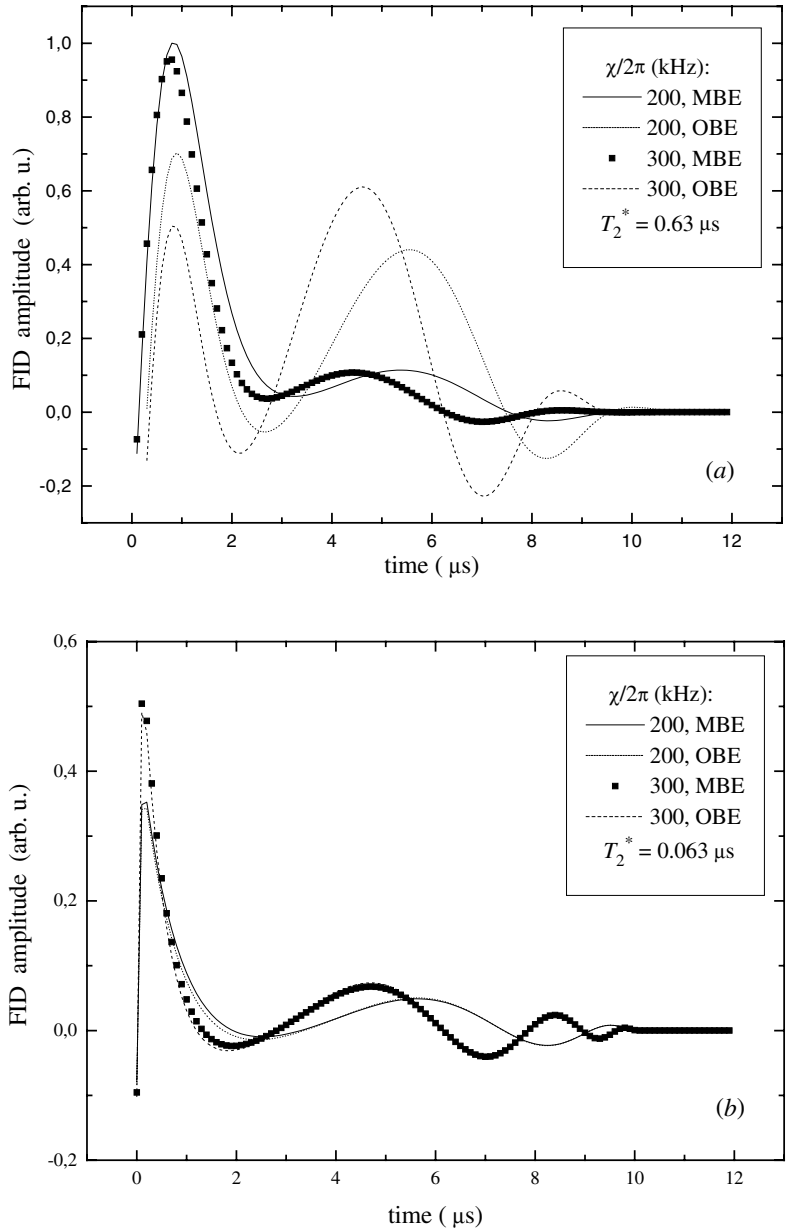

Figure 6. Oscillatory FID responses for $T_2^* = 0.63$ μs (*a*) and $T_2^* = 0.063$ μs (*b*). $\chi/2\pi = 200$ and 300 kHz, $t_p = 10$ μs.

Perhaps because of the periodic dependence of the signal on the pulse area, the maximum and decay rate are varied with t_p alternately. For $t_p \geqslant 100$ μs, the signal monotonically tends from above to the steady-state prepared FID, the decreasing part of which is a single exponential function of time (full curve). The intensity of this signal at its maximum is greater by 15 dB than that for the analogous signal calculated in the OBE model (line–symbol curve in figure 5). With increasing χ this difference increases. In obtaining these and other

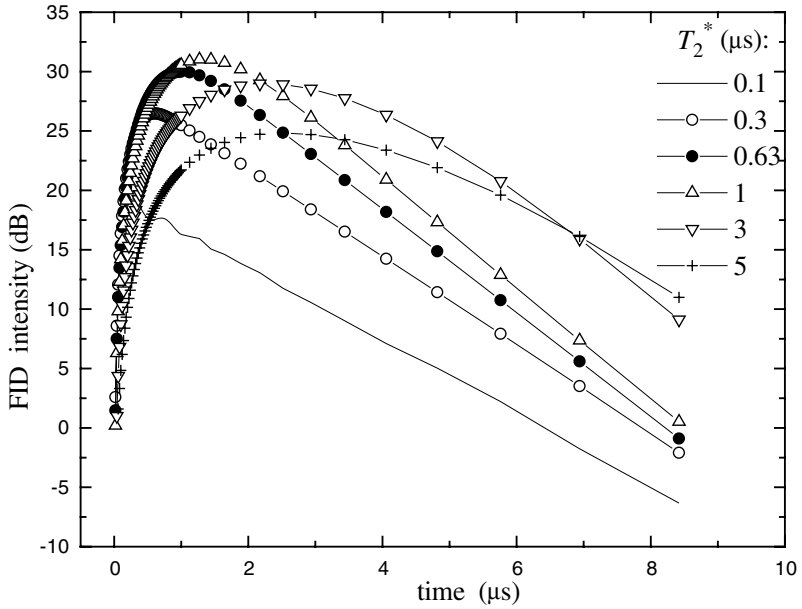

Figure 7. Calculated responses of steady-state prepared FID at $\chi = 2\pi \times 54$ kHz for different values of reversible relaxation time $T_2^* = \sigma^{-1}$.

results below, the following values of the parameters were used: $a_\omega = 3 \times 10^{-8}$ cm^{-3} c^{-1}, $a_\Gamma = 2.76 \times 10^{-8}$ cm^{-3} c^{-1}, $r^2 = 2 \times 10^{-9}$ c^2, $T_1 = 5 \times 10^{-3}$ c, $T_2 = \Gamma_0^{-1} = 7.5 \times 10^{-5}$ c, $n_0 = 4 \times 10^{16}$ cm^{-3} and, excepting figures 6 and 7, $\sigma = 2\pi \times 0.25$ MHz.

In the case of large pulse area, $\chi t_p \geqslant 2\pi$, one needs again to compare predictions of the OBE and MBE models since strong driving field can significantly change the dispersion and damping parameters. Examples of the oscillatory decay for $\chi t_p = 4\pi$, 6π and pulse length $t_p = 10$ μs are depicted in figure 6(a) for $\sigma = 2\pi \times 0.25$ MHz ($T_2^* = 0.63$ μs) and in figure 6(b) for $T_2^* = 0.063$ μs. It is seen that in figure 6(a) the oscillations in the MBE model are more damped than those in the OBE model. In the case of larger inhomogeneous width (figure 6(b)), there is no significant difference between signals in the two models. That is, here the signal behaviour is mainly determined by the large inhomogeneous width and not by the homogeneous one. Note that in the system with large inhomogeneous line width the signal lasts strongly for period t_p, in agreement with [23]; at lower values of σ the oscillatory response somewhat extends to times $t > t_p$. In figure 6(a) (small σ) the first maximum of the FID amplitude decreases with increasing χ, while in figure 6(b) (large σ) the opposite is observed.

For different samples used in experiments [4–6] a broad range of inhomogeneous line width is characteristic. Hence, it is useful to consider the FID dependence on this parameter though other parameters for the samples are unknown. The FID responses for several values of the reversible relaxation time T_2^* are shown in figure 7 for the case of steady-state excitation with $\chi = 2\pi \times 54$ kHz. Solid circles in the figure again correspond to $\sigma = 2\pi \times 0.25$ MHz ($T_2^* = 0.63$ μs) and represent an exact copy of the experimental curve in figure 1 of [5] with decay rate $\Gamma = 2\pi \times 78$ kHz. For small values of T_2^* (solid line in the figure), the initial part of the decay has an oscillatory character. For a given value of χ, the maximum of the FID response initially rises with increasing T_2^*, then decreases, having a stable tendency to broadening.

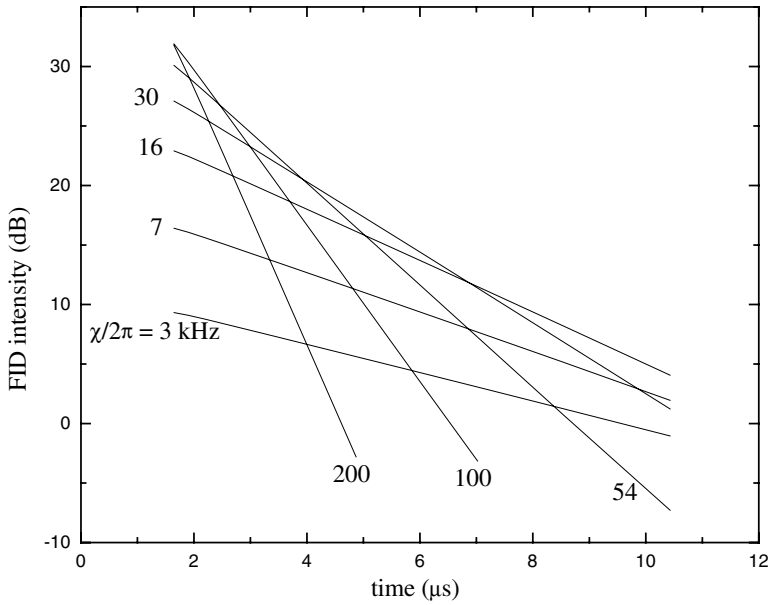

Figure 8. Decaying part of steady-state-prepared FID signals for different values of the Rabi frequency.

In the whole range of experimentally available values of χ [5], the decreasing part of the FID prepared by steady-state excitation is a single exponential function (similar to the curve with solid circles in figure 7) with power-dependent decay rate, as shown in figure 8.

From the time dependence of the FID similar to that shown in figure 8, we have determined the decay rate, $\Gamma(\chi)$, for a set of values of χ. The open circles in figure 9 depict the dependence obtained in such a way. Experimental results of Boscaino and La Bella [5] (up triangles), the theoretical dependence [5, 24]

$$\Gamma = (1/T_2)\lfloor 1 + (1 + \chi^2 T_1 T_2)^{1/2} \rfloor \tag{17}$$

following from the OBE (solid squares), and that of the Redfield theory in the high-field limit

$$\Gamma = \chi/\sqrt{2} \tag{18}$$

(solid circles) are also shown in this figure. One sees that $\Gamma(\chi)$ obtained here numerically from equations (1) with $\Gamma_{2u}(\chi)$ and $\Gamma_{2v}(\chi, t)$, for small fields follows the OBE result; at 4 kHz $\leqslant \chi/2\pi \leqslant$ 20 kHz it undergoes a crossover from the Bloch to the Redfield regime; with further increasing χ asymptotically tends to the Redfield limit and in the whole range of measurements coincides very well with experiment [5].

There is a need to specify a peculiarity in the free induction decay. The irreversible damping of the FID response is given by the exponential factor in equations (15). Since $\Gamma_{2v}(\chi) > \Gamma_0$ (as is seen, for example, from figure 4), the more *faster* decay in the present MBE model was to be expected, contrary to the experiment, than in the ordinary Bloch one. Curves 1 and 2 in figure 10 show the decay at $\chi = 2\pi \times 100$ kHz in the present model: curve 1 is without considering the exponential factor in equations (15) and curve 2 is with that factor. Similarly, curves 3 and 4 present the FID decay in the OBE model: curve 3 is without considering the exponential factor with $T_2 = \Gamma_0^{-1} = 7.5 \times 10^{-5}$ s and curve 4 is with that factor. It is seen that the role of irreversible damping in the OBE model is negligible and the

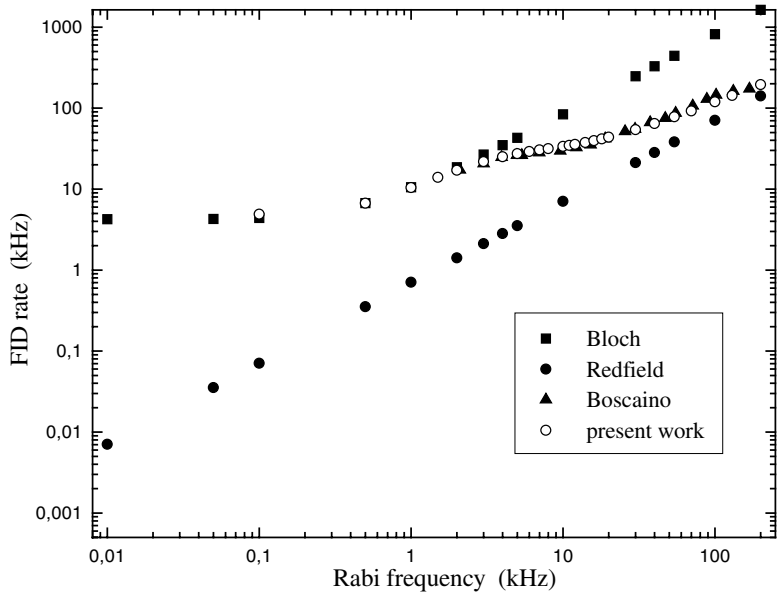

Figure 9. Calculated FID rate, $\Gamma/2\pi$, versus Rabi frequency, $\chi/2\pi$, for sample no 1 of [5] (open circles). Solid squares and solid circles are the theoretical dependences expected from the ordinary Bloch theory (17) and from the Redfield one (18) respectively. Solid triangles are experimental data of Boscaino and La Bella [5].

decay process is mainly determined by the reversible dephasing of the coherent state produced during the steady-state excitation. In our MBE model, too, though the large irreversible damping somewhat influences the decay (compare curves 1 and 2), the last is mainly governed by the coherent state formed during the steady-state excitation. Figure 10 shows that this state is essentially different for two models considered. It is important that parameter $T_{2u}(\chi)$, which in the TN is of no any importance, has a significant impact on the steady-state formation. In particular, the initial value of the dispersion, $u^{(0)}$, which mainly determines the FID signal, is proportional to $T_{2u}(\chi)$ (see expressions (14)).

5. Discussion and conclusions

Since the first experiments on the electron spin echoes (ESEs) in solids, it was established that they cannot be explained in the framework of the OBE. The discrepancy between experiment and theory rises with increasing driving-field intensity (see, for example, [19, 20]). As we see above, the same is true for other related transient effects in solids, namely TN and FID. Finally, there is much work on the same transient effects in optics with the same conclusion.

Beginning with the famous paper by Klauder and Anderson [16], various statistical theories of the above transient effects were elaborated. In particular, the mechanisms of spectral diffusion (SD) and of instantaneous diffusion (ID) [16] are widely used to explain the various and complicated relaxation processes in those fields.

Although there is no any doubt in the existence of SD and ID, in our opinion the interpretation of the ID mechanism as a relaxation one only is incomplete. As is shown earlier [25], in addition to the usual nonlinear excitation mechanism of the echo-formation, the ID mechanism is a source of two new nonlinear ones, namely the intensity-dependent

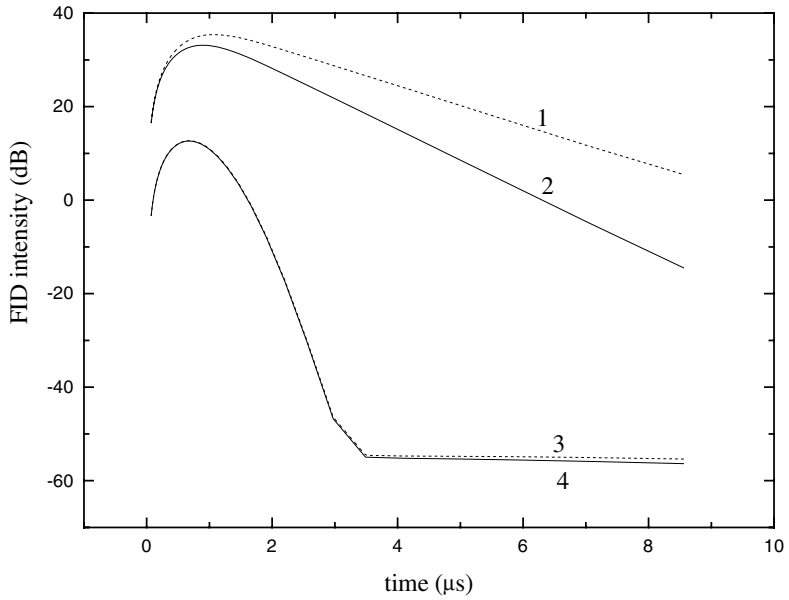

Figure 10. Calculated FID response in the present MBE model (curves 1, 2) and in the OBE model (curves 3, 4): curves 1 and 3 are without considering the exponential factor in equations (15) and those 2 and 4 are with that factor (with $T_2 = \Gamma_0^{-1} = 7.5 \times 10^{-5}$ s for the OBE model). $\chi = 2\pi \times 100$ kHz.

dispersion and intensity-dependent damping. Phenomenological expressions (8) for $\Delta\omega(t)$ and (12) for $\Gamma_{2v}(t)$ present the ID mechanism in the TN effect and those with $t = t_p$ (and, in particular, with $t_p \to \infty$) in the FID effect. In summary, we conclude that the meaning of the ID mechanism consist in coherent variation of the spin components by a coherent driving field ('instantaneous' in the pulse-echo experiments and more or less continuous in transient nutations, for example); the variation of longitudinal components, m_z, leads to the intensity-dependent dispersion and that of transverse ones manifests itself as the intensity-dependent damping. Moreover, the above noted *nonlinear excitation mechanism* is a consequence of the ID mechanism as well since it consist in the nonlinear, in fact, interaction of the driving field with the *coherently varied* transverse spin components.

It is worth noting that unlike the common statements that the ID mechanism acts during the excitation pulses, in the echo-formation process the power-dependent dispersion, $\Delta\omega(t)$, is *formed* during the excitation pulses but *acts* as nonlinear mechanism (as a source of the power- and time-dependent coherent phase) between and after the pulses (see also note on parameter a_ω below).

Returning to the concrete results in the two preceding sections, it is clear why the TN decay is faster than expected from the OBE model. Indeed, the Redfield slowing down described by Γ_{2u} affects the dispersive component $U(t) \sim 0$ only, while damping of the absorptive component $V(t)$ (and, really, of the whole response) is governed by large and intensity-dependent $\Gamma_{2v}(\chi, t)$. Referring to figures 1, and 3 or 4, we see that there is a significant difference in magnitude and behaviour of $\Gamma_{2v}(\chi, t)$ and $\Gamma(\chi)$. While $\Gamma_{2v}(\chi, t)$ increases in an oscillatory manner to value $\Gamma_{2v}(\chi, t_p) > \Gamma(\chi)$ during the excitation, the intensity-dependent TN decay rate $\Gamma(\chi)$ is constant in time.

Results of section 4 show the importance of the preparative stage both in pulse and steady-state prepared FID. In the last case, as we already pointed out in the preceding section, the

decay is mainly determined by the steady-state preparation stage where parameter $T_{2u}(\chi)$ is of more importance than $\Gamma_{2v}(\chi, t)$.

As a summary to figures 4 and 9, we have to say that the TN and FID give somewhat different information about irreversible damping in the system.

We call attention to the large difference in the magnitude of parameter a_ω in the two processes: $a_\omega = 1.78 \times 10^{-9}$ cm^{-3} s^{-1} in the TN process, and 3×10^{-8} cm^{-3} s^{-1} for the FID effect. This is caused by the circumstance that the z-component of the Bloch vector in the TN process experiences fast oscillations averaging the intensity-dependent shift of the resonance frequency. On the other hand, in the FID effect $w = w^{(0)}$ is time independent and hence the shift is effective.

Very good agreement between the solutions of the MBE based on intensity-dependent parameters (5), (8), (9) or (10) and (12), and experimental results on TN [2] and on FID [5] unambiguously confirms the correctness of those parameters and MBE (1) in general. In particular, results of figures 3 and 4 show that power-dependent damping (12) as the ID mechanism is decisive in the TN effect. On the other hand, we can say that expressions (9) or (10) and the first term in the right-hand side of (12) correctly describe the possible contribution of the SD mechanism.

In conclusion, we have presented a modified version of the Bloch equations with specific power-dependent relaxation and dispersion parameters. These parameters take into account the contributions of both the instantaneous and spectral diffusion mechanisms. Further, analytic and numerical solutions of MBE are applied to the detailed experiments by Boscaino *et al* on EPR transient nutations and free induction decay in solids. Good quantitative agreement between the theory and experiments is obtained in whole range of experimentally available field intensities and several parameters contained in the theory are estimated. In the framework of MBE, we have theoretically considered also properties of the oscillatory FID which, to our knowledge, has yet to be observed in EPR.

References

[1] Boscaino R, Gelardi F M and Mantegna R N 1987 *Phys. Lett.* A **124** 373
[2] Boscaino R, Gelardi F M and Korb J P 1993 *Phys. Rev.* B **48** 7077
[3] Agnello S, Boscaino R, Cannas M, Gelardi F M and Shakhmuratov R N 1999 *Phys. Rev.* A **59** 4087
[4] Boscaino R, Gelardi F M and Messina G 1983 *Phys. Rev.* A **28** 495
[5] Boscaino R and La Bella M V 1990 *Phys. Rev.* A **41** 5171
[6] Boscaino R and Gelardi F M 1992 *Phys. Rev.* A **45** 546
[7] Torrey H C 1949 *Phys. Rev.* **76** 1059
[8] Hahn E L 1950 *Phys. Rev.* **77** 297
[9] Bloch F 1946 *Phys. Rev.* **70** 460
[10] De Voe R G and Brewer R G 1983 *Phys. Rev. Lett.* **50** 1269
[11] Szabo A and Muramoto T 1989 *Phys. Rev.* A **39** 3992
[12] Wodkiewicz K and Eberly J H 1985 *Phys. Rev.* A **32** 992
[13] Berman P R and Brewer R G 1985 *Phys. Rev.* A **32** 2784
[14] Malinovsky V S and Szabo A 1997 *Phys. Rev.* A **55** 3826
[15] Shakhmuratov R N, Gelardi F M and Cannas M 1997 *Phys. Rev. Lett.* **79** 2963
[16] Klauder J R and Anderson P W 1962 *Phys. Rev.* **125** 912
[17] Redfield A G 1955 *Phys. Rev.* **98** 1787
[18] Tomita K 1958 *Prog. Theor. Phys.* **19** 541
[19] Boscaino R and Gelardi F M 1992 *Phys. Rev.* B **46** 14 550
[20] Boscaino R, Gelardi F M and Cannas M 1996 *Phys. Rev.* B **53** 302
[21] Schenzle A, Wong N C and Brewer R G 1980 *Phys. Rev.* A **21** 887
[22] Kunitomo M, Endo T, Nakanishi S and Hashi T 1982 *Phys. Rev.* A **25** 2235
[23] Schenzle A, Wong N C and Brewer R G 1980 *Phys. Rev.* A **22** 635
[24] DeVoe R G and Brewer R G 1979 *Phys. Rev.* A **20** 2449
[25] Asadullin Ya Ya 1993 *J. Phys.: Condens. Matter* **5** 3689